Dual Biochemically Breakable Drug Carriers from Programmed Telechelic Homopolymers

Adrian Moreno,[†] Ana Jiménez-Alesanco,[‡] Juan C. Ronda,[†] Virginia Cádiz,[†] Marina Galià,[†]

Virgil Percec,[§] Olga Abian,[‡,O,^,‖,∇] and Gerard Lligadas*[,†,§]

[†] *Laboratory of Sustainable Polymers, Department of Analytical Chemistry and Organic Chemistry, University Rovira i Virgili, Tarragona 43007, Spain*

[‡] *Institute of Biocomputation and Physics of Complex Systems (BIFI), Joint Units IQFR-CSIC-BIFI, and GBsC-CSIC-BIFI, Universidad de Zaragoza, Zaragoza, Spain*

[§] *Roy & Diana Vagelos Laboratories, Department of Chemistry, University of Pennsylvania, Philadelphia, Pennsylvania 19104-6323, United States*

[O] *Instituto Aragonés de Ciencias de la Salud (IACS), Zaragoza, Spain*

[^] *Instituto de Investigación Sanitaria de Aragón (IIS Aragon), Zaragoza, Spain*

[‖] *Centro de Investigación Biomédica en Red en el Área Temática de Enfermedades Hepáticas Digestivas (CIBERehd), Madrid, Spain*

[∇] *Departamento de Bioquímica y Biología Molecular y Celular, Universidad de Zaragoza, Zaragoza, Spain*

ABSTRACT: Well-defined hydrophilic telechelic dibromo poly(triethyleneglycol monomethyl ether acrylate)s were prepared by single-electron transfer living radical polymerization employing a hydrophobic difunctional initiator containing acetal and disulfide linkages. Despite the resulting homopolymers contain small hydrophobic contents (< 8.5 wt.-% of the entire structure), they are able to self-assemble in water into nanoscale micelle-like particles *via* chain-folding. Acetal and disulfide linkages were demonstrated to be "keystone" units for their dual stimuli-responsive behavior under biochemically relevant conditions. Their site-selective middle-chain cleavage under both acid pH and reductive conditions splits the homopolymer into two equally-sized fragments and results in the breakdown of the nanoassemblies. The drug loading/delivery potential of theses nanoparticles was investigated using curcumine combining *in vitro* drug release, cytotoxicity and cellular uptake studies with human cancer cell lines (HT-29 and HeLa). Importantly, this strategy may be extended to prepare innovative nanoplatforms based on hydrophilic homo- or random copolymers for intelligent drug delivery.

Keywords: amphiphilic homopolymer, stimuli-responsive, SET-LRP, nanocarrier, self-assembly

INTRODUCTION

Amphiphilic polymer design represents a captivating class of biorelevant templates on account of their ability to form in aqueous media a range of different nanoassemblies such as spherical micelles, vesicles, and cylinders.[1-5] Despite most of these self-organized structures rely on block copolymers, the self-directed assembly of amphiphilic homopolymers represents a promising direction to give rise to high-order morphologies in solution, greatly benefiting from the common easier synthetic accessibility of their precursors.[6,7] Making the most of key advances in controlled/living polymerization methods, associative homopolymers are classically based on amphiphilically equipped monomers (Scheme 1A) [8-12] or alternatively consist of well-defined fully hydrophilic homopolymers with one or two hydrophobic end-group(s) (Scheme 1B). [13-17] Mimicking conventional amphiphilic block copolymers, their homopolymer analogues also can form micellar,[18,19] vesicular,[20,21] and related aggregates in water as well as reverse structures in non-polar solvents.[22,23]

Meanwhile, over the past several years, interest in gaining precise control over solution-state self-assembled polymer morphologies has exploded leading to a huge variety of macromolecular architectures which enable stimuli-induced morphological changes, e.g. volume expansion, or transitions, e.g. micelles to vesicles. [5,24-26] In this regard, for many biological applications, e.g. drug delivery and imaging, the development of nanoassemblies, which are designed to undergo a complete breakdown and release cargo(s) in response to external stimuli, is highly desirable and represent an ultimate goal.[27-29] Acid pH,[30] temperature,[31] light,[32] redox potential,[33] among others, are typical stimuli that have been extensively explored. However, dual or multi stimuli-breakable systems are even more advantageous to make the release process more efficient, accurate, and controllable.[34,35]

Scheme 1. Schematic Representation of the Synthetic Pathways to Amphiphilic Homopolymers. Color code: blue as hydrophilic and water-soluble, green as hydrophobic and water-insoluble and red as stimuli-cleavable linkage(s).

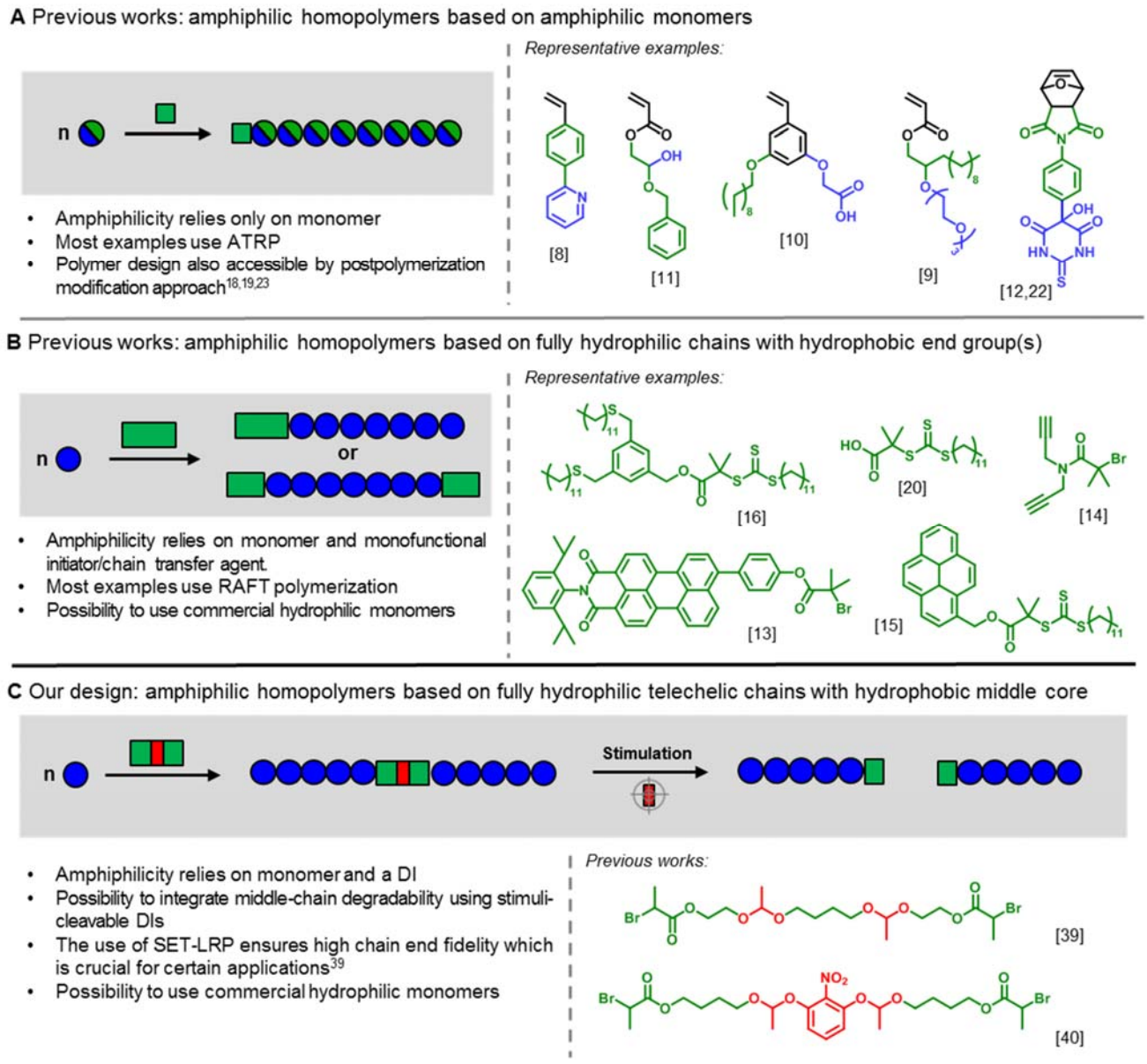

Previously, we have shown that fully hydrophilic telechelic dibromo polymers prepared by combining single-electron transfer living radical polymerization (SET-LRP)[36-38] with hydrophobic difunctional initiators (DIs) is a convenient means of synthesizing associative telechelic homo or random polymers with predicted molecular weight, narrow polydispersity, and high chain-end functionality

(Scheme 1C).[39,40] Aqueous self-assembly of these amphililic homopolymers results in initiator residue incorporation at the hydrophobic core of micelle-like nanoassemblies *via* chain-folding. This amphiphilic homopolymer design is especially attractive in terms of control over disassembly process because chemical engineering of DI enables to program a predetermined degradation code by introducing labile linkages into its design. The use of hydrophobic DIs containing cleavable functions enables reduction of the number-average molar mass (M_n) by half after degradation which dramatically modifies amphiphilic balance (Scheme 1C),[41,42] further resulting in the breakdown of the nanoassemblies.[39,40]

Herein, we report a facile strategy to prepare dual pH and reduction breakable micelle-like nanoassemblies, formed from the self-directed assembly of fully hydrophilic poly(triethyleneglycol monomethyl ether acrylate)s [poly(TEGA)s] prepared *via* SET-LRP employing a hydrophobic DI integrating acetal and disulfide cleavable linkages as a double dual "keystone" units. Although dual acidic pH/reduction-responsive degradable block copolymer systems have received increasing attention for cellular delivery applications by means of increased acidity and glutathione (thiol) concentration of tumor cells or tissues compared to the healthy ones, [35,43-45] this is the first example of homopolymer that behaves the same way as amphiphilic block copolymers. Despite containing a low hydrophobic fraction of hydrophobic initiator residue (< 8.5 wt.-%), the synthesized homopolymers were able to self-assemble in aqueous solution and encapsulate hydrophobes into their core. We vividly demonstrated the dual capability of the conceived assemblies to swell and finally breakdown under biochemically relevant conditions, i.e. weakly acidic and/or reductive environment, owing to the site-selective middle-chain cleavage of acetal and/or disulfide units. Additionally, the potential of these amphiphilic homopolymers for effective loading and delivering anti-cancer drugs has been tested using curcumine (CC) as a model hydrophobic drug.

EXPERIMENTAL SECTION

TEGA Monomer Synthesis. Triethylene glycol monomethyl ether (25 g, 0.15 mol) and anhydrous TEA (31 mL, 0.20 mol) were dissolved in anhydrous Me-THF (60 mL) under a positive flow of argon. Then, the solution was placed in an ice-bath (0-5 °C) and allowed to stir for 30 min. before starting the addition of acryloyl chloride (18 mL, 0.22 mol) dissolved in Me-THF (20 mL). The reaction was then allowed to proceed for 24 h at room temperature. After that, the crude mixture was filtered and the excess of Me-THF was removed under reduced pressure. The final residue was purified by vacuum distillation, in the presence of 5 (w/w %) of hydroquinone, to afford TEGA (23.6g, 83%) as a colorless viscous liquid. ^{1}H NMR analysis was consistent with previous reports.[46]

General Procedure for SET-LRP. This procedure is representative for all the polymerizations conducted herein. The SET-LRP of TEGA using $DI_{A/R}$ as initiator in DMSO under the following conditions: $[TEGA]_0/[DI_{A/R}]_0/[Me_6\text{-TREN}]_0$ = 50/1/0.2 is described. Initiator $DI_{A/R}$ (34 mg, 1 mmol) was dissolved in DMSO (0.25 mL) and charged in a 25 mL Schlenk flask together with TEGA monomer (0.5 mL, 2.3 mmol) and Me_6-TREN ligand (2.6 μL, 0.2 mmol). Next, oxygen was removed from the reaction mixture by six consecutive freeze-pump (1 min)-thaw (F-T-P) cycles. After that, a piece of surface-activated copper wire (4.5 cm), coil wrapped around a Teflon-coated magnetic stir bar, was introduced into the flask under a strong flow of argon and held above the reaction mixture using an external neodymium magnet. Two F-P-T cycles were applied and after that, the reaction mixture was placed in a thermostat bath at 25 °C. The introduction of the magnetic stir bar into the reaction vessel started the polymerization process (t = 0). In general, the reactions were allowed to proceed for 2 h, and only for kinetic experiments, monomer conversion was determined by periodic withdrawing of samples at different times through the side arm of the tube previously purged with argon using an Hamilton gastight syringe. The collected samples were dissolved and analyzed by ^{1}H-NMR to determine the monomer conversion followed by solvent

evaporation to determine the molecular weight by GPC. The final polymer was purified before any further study by passing the diluted (THF) crude solution through a short basic alumina column to remove copper salt residues and subsequently by dialysis against acetone (Yield 85-89%). Poly(Triethylene glycol monomethyl ether acrylate) (ATHs): ^{1}H NMR (400 MHz, $CDCl_3$, δ) = 4.7 (q, 2H), 4.34-4.15 (m, 6H), 3.8 (dd, 4H), 3.6-3.5 (m, 8H), 3.4 (s, 6H), 2.8 (m, 4H), 2.5-1.5 (m, 18H), 1.35 (d, 6H), 1.13 (m, 6H); ^{13}C NMR (100.6 MHz, $CDCl_3$, δ) = 170.04, 160.98, 99.83, 70.55, 65.34, 63.71, 63.06, 61.89, 52.65, 39.79, 39.27, 36.64, 32.45, 26.69, 21.62, 19.68.

General Procedure to Conduct Middle-Chain Cleavage of Amphiphilic Telechelic Homopolymers (ATHs). A solution of ATH (50 mg) in THF (2 mL) was introduced in a 5 mL round-bottomed flask equipped with a magnetic stir bar. After that, TFA (80 µL, 0.1 M in THF), for acid cleavage, or PBu_3 (200 µL, 100 equiv.), for reductive cleavage, was added and the resulting reaction mixture was allowed to stir during 1 hour at room temperature under argon atmosphere. The reaction mixture was passed through a short basic alumina column prior the GPC analysis.

Self-Assembly of ATHs and CC-Loading. ATH nanoassemblies were prepared by two different procedures: nanoprecipitation (solvent-switch method) and direct dispersion in water. Nanoprecipitation method was conducted as follows. First, 10 mg of ATH were dissolved in 1 mL of THF. To this solution 7 mL of Milli Q water was added progressively at a rate of 15 $\mu L \cdot min^{-1}$ in a total of 7 hours using a syringe pump from Thermo Fisher Scientific. The excess of THF was removed by dialysis against PBS (pH = 7.4) during 1 day using a dialysis membrane with a MWCO of 2000 kDa. The final mixture was diluted to 10 mL using phosphate buffer solution to reach a final concentration of 1 $mg \cdot mL^{-1}$. Self-assembly by direct dispersion was conducted by simply mixing ATH and water at 1 $mg \cdot mL^{-1}$. The preparation of CC-loaded nanoassemblies was conducted as follows: ATH (10 mg) and CC (1.2 mg) were dissolved in THF (1 mL) and Milli Q water was progressively added to the organic solution following the above described

nanoprecipitation methodology. After that, the unencapsulated CC was removed by filtering the solution through a nylon membrane (0.45 μm). The drug loading content (DLC) and encapsulation efficiency (EE) values were determined by freeze drying the CC-loaded nanoassemblies solution followed by re-dispersion in acetone and analysis by fluorescence emission spectra at 517 nm using a standard calibration curve. The DLC and EE values were calculated according the following equation: DLC (%) = (weight of drug loaded in nanoassemblies)/(weight of nanoassemblies) x100, and EE (%) = (amount of loaded drug)/(total amount of feeding drug) x100.

Determination of Critical Aggregation Concentration (CAC). The CAC was determined using NR as fluorescent probe by direct monitoring the emission changes in peak at 617 nm. Fluorescence emission spectra were recorded fixing the excitation wavelength at 550 nm at an emission range of 560-720 nm. The concentration of AHPs were varied from 1.0 x 10^{-9} to 1.0 mg·mL^{-1} and the NR concentration was fixed at 6.7 x 10^{-7} M.

pH-Triggered Release of CC from CC-Loaded Nanoassemblies. The release of CC was investigated at 25 °C under the following conditions: pH 7.4 (control), pH 7.0, pH 6.0 and pH 5.0. First, CC-loaded ATH1 nanoassemblies were prepared by nanoprecipitation method as described above. Next, the CC-loaded nanoassemblies solutions at pH 7.4 was adjusted to pH 7.0, 6.0 and 5.0 using a buffer solution at pH 1.0. The release of the CC was tracked by monitoring the time evolution of fluorescence emission intensity of CC-loaded nanoassemblies (CC, λ_{ex} = 430 nm, λ_{em} = 516 nm).

Reductive-Triggered Release of CC from CC-Loaded Nanoassemblies. The release of CC was investigated at 25 °C under different concentrations of DTT: 5.0 mM, 10.0 mM, and 15.0 mM. First, CC-loaded ATH1 nanoassemblies were prepared by a nanoprecipitation method as described above. Next, micellar solutions containing 5.0 mM, 10.0 mM, and 15.0 mM DTT were obtained by the addition of the required amount of aqueous DTT solution (0.1 M) to reach the targeted concentration. The release of the

CC was tracked by monitoring the time evolution of fluorescence emission intensity of CC-loaded nanoassemblies (CC, λ_{ex} = 430 nm, λ_{em} = 516 nm).

Dual Stimuli-Triggered Release of CC from CC-Loaded Nanoassemblies. The release of CC was investigated by applying sequential and additive reductive and acid treatments. First, the colloidal dispersion of CC-loaded ATH1 nanoassemblies (pH 7.4) was adjusted to 15 mM DTT as described above. After 3 h, the pH of the solution was adjusted to pH 5.0 to submit the release process under co-triggered conditions. The release of CC was tracked by monitoring the time evolution of fluorescence emission intensity of CC-loaded nanoassemblies (CC, λ_{ex} = 430 nm, λ_{em} = 516 nm).

Cell Viability Assays. Cellular cytotoxicity was assessed in two human cancer cell lines: HT-29 and HeLa cells. The cell viability experiments were carried out in three conditions: cells in presence of blank ATH1 polymer as control, CC-loaded ATH1 nanoassemblies and free CC. Cells were plated in 96-well plates (8,000 cells/100 µl/well in HeLa cells; 9,000 cells/100 µl/well in HT-29 cells) with supplemented DMEM without phenol red. After 24 h, several serial dilutions of the polymer and CC were added to the cells. 300 µg/ml was the maximum tested concentration of ATH1 and 16.8 µg/ml in the case of CC. The cells were incubated in presence of the compounds during 48 hours and after this period the cytotoxicity were checked by adding the CellTiter reagent. The CellTiter 96® AQueous One Solution Cell Proliferation Assay Kit (Promega, Madrid, Spain) provides a convenient and sensitive procedure for determining the number of viable cells in cytotoxicity assays. 20 µl of CellTiter reagent (1/4 dilution in DMEM without phenol red) were added into each well of the 96-well assay plate containing the samples. The plate was incubated at 37 °C for 2 h in a humidified, 5% CO_2 atmosphere and later the absorbance was recorded using the Synergy HT (BioTek) plate reader and the Gen5 1.10 software at 490 nm (reference wavelength: 800 nm). Each experiment was performed in triplicate and repeated at least two times.

Cell Uptake Studies. The cellular uptake of CC was studied toward HeLa and HT-29 cells using fluorescence microscopy. Cells were seeded in a 24-well culture plate at a density of 80,000 cells/500 μl/well in the case of HeLa cells and 90,000 cells/500 μl/well in the case of HT-29 cells. After 24 h of culture, the cells were treated with polymer, CC-loaded nanoassemblies or free CC for 24 h. The maximum concentration of polymer was 120 μg/ml and 6.72 μg/ml in the case of curcumin. During this incubation, cells were monitored continuously under a confocal microscope. Images were taken every 30 minutes during 24 hours by employing both bright field microscopy and the GFP fluorescence filter. Each experiment was repeated at least three times.

RESULTS AND DISCUSSION

Preparation and Characterization of ATHs. The high degree of structural control and chain-end fidelity enabled by SET-LRP allows the preparation of well-defined telechelic dibromo polymers featuring single[47] and multiple[42] cleavage units at the chain center by using cleavable DIs.

Herein, amphiphilic telechelic homopolymers [poly(TEGA)s, ATH1-3, see Figure 1A] consisting of two fully hydrophilic and water-soluble blocks connected by a monodisperse, hydrophobic, and dual cleavable initiator residue, were synthesized using the sequence-encoded α-haloester-type initiator $DI_{A/R}$ (Figure 1A). Surface-activated copper wire was used as unique metal source and tris[2-(dimethylamino)ethyl]amine (Me_6-TREN) as a disproportionation-favoring ligand to conduct SET-LRP in DMSO.[48] The ratio of TEGA monomer to initiator was varied from 25 to 120 to yield symmetric homopolymers with increasing chain lengths while retaining a low weight percentage of the hydrophobic initiator residue (< 8.5 wt %). The polymerization results are presented in Table 1.

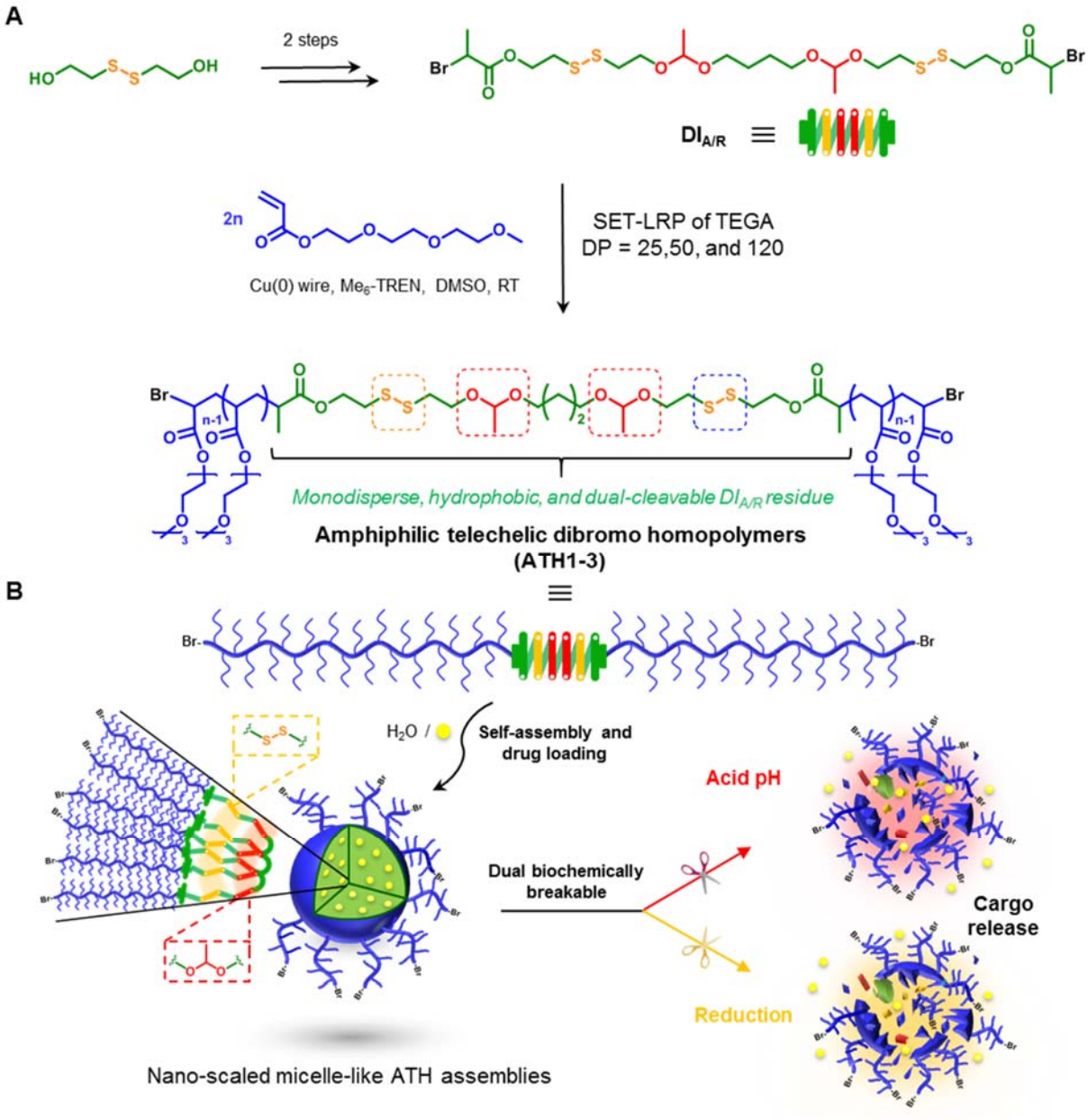

Figure 1. Schematic illustrating design and construction of dual biochemically breakable micelle-like nanocarriers *via* self-assembly of programmed fully hydrophilic TEGA homopolymers: (A) Synthesis of $DI_{A/R}$ as hydrophobic initiator containing double acetal and disulfide linkages and subsequent SET-LRP synthesis of ATH1-3 homopolymers from TEGA monomer using copper wire and Me_6-TREN in DMSO at 25 ºC. (B) Aqueous self-assembly of ATH1-3 into pH and reduction dual responsive micelle-like nanocarriers for hydrophobic drugs. Color code: blue as hydrophilic and water-soluble, green as hydrophobic and water-insoluble, red as acidic pH-sensitive acetal linkages, and orange as reduction-sensitive disulfide linkages. Detailed synthesis and characterization of $DI_{A/R}$ is available in an earlier work (see Figures S1-3).[42]

Table 1. Characterization of the TEGA Homopolymers and Their Self-Assembly Parameters in Aqueous Media.

ATH [a]	DP [b]	Conv.[c] (%)	M(th)[d] (Da)	M_n[e] (Da)	M_w/M_n[e]	M_n[f] (Da)	DIR[g] (wt%)	D_z[h] (nm)	PDI[h]	D_z[i] (nm)	PDI[i]	CAC[j] (mg·L^{-1})
1	25	91	5400	6400	1.23	5700	8.4	5 ± 1	0.29 ± 0.06	79 ± 4	0.13 ± 0.02	1.7
2	50	95	10230	11010	1.24	10800	5.0	6 ± 2	0.29 ± 0.08	127 ± 2	0.15 ± 0.03	2.1
3	120	87	26190	30500	1.25	24700	1.8	4 ± 2	0.34 ± 0.03	175 ± 5	0.21 ± 0.03	4.3

[a] Polymerization conditions: TEGA = 0.5 mL, DMSO = 0.25 mL, and $[DI_{A/R}]_0/[Me_6\text{-TREN}]_0$ = 1/0.2 using 4.5 cm of hydrazine-activated copper wire 20 gauge at 25 ºC for 2 h. [b] Calculated from the $[TEGA]_0/[DI_{A/R}]_0$ ratio. [c] Determined by ^{1}H NMR. [d] M(th) = 218.2 × $[TEGA]_0/[DI_{A/R}]_0$ × conv. + 720.6. [e] Determined by GPC in THF using PMMA standards. [f] Determined by ^{1}H NMR. [g] Weight fraction of the hydrophobic initiator residue in the whole hydrophilic ATH. [h] DLS results of solutions in $CHCl_3$ at 20 mg·mL^{-1} (25 ºC) presented as the mean ± standard deviation of three replicates. [i] DLS results of colloidal solutions in water at 1 mg·mL^{-1} (25 ºC) presented as the mean ± standard deviation of three replicates. [j] Critical aggregation concentration determined by fluorescence spectroscopy using Nile Red as a probe.

SET-LRP reactions at 25 ºC were fast, reaching up to ≈ 90 % conversion within 2 h. A representative kinetic study targeting a degree of polymerization (DP) of 50 (25 for each two initiating sites) revealed that the homopolymerization of TEGA proceeded controlled, as all features of a living polymerization kinetics were indeed displayed, e.g. linear semi-logarithmic kinetic plot and good agreement between measured M_n^{GPC} and the theoretical M(th) values are retained up to high conversion (Figure 2A). After synthesis, the three produced ATHs (ATH1-3) were first purified before any further study by passing the diluted (THF) crude solution through a short basic alumina column to remove copper salt residues. Next, the eluate was exhaustively dialyzed against acetone (2.0 kDa MWCO) to remove residual monomer and furnish sticky clear solids once concentrated. GPC analysis revealed relatively narrow peaks (M_w/M_n < 1.25) and confirmed that molecular weight of ATHs increased from ATH1 to ATH3 while agreeing well with targeted values (Table 1). The structure of the synthesized ATHs was further characterized by ^{1}H NMR spectroscopy as depicted in Figure 2B and Figures S4,5.

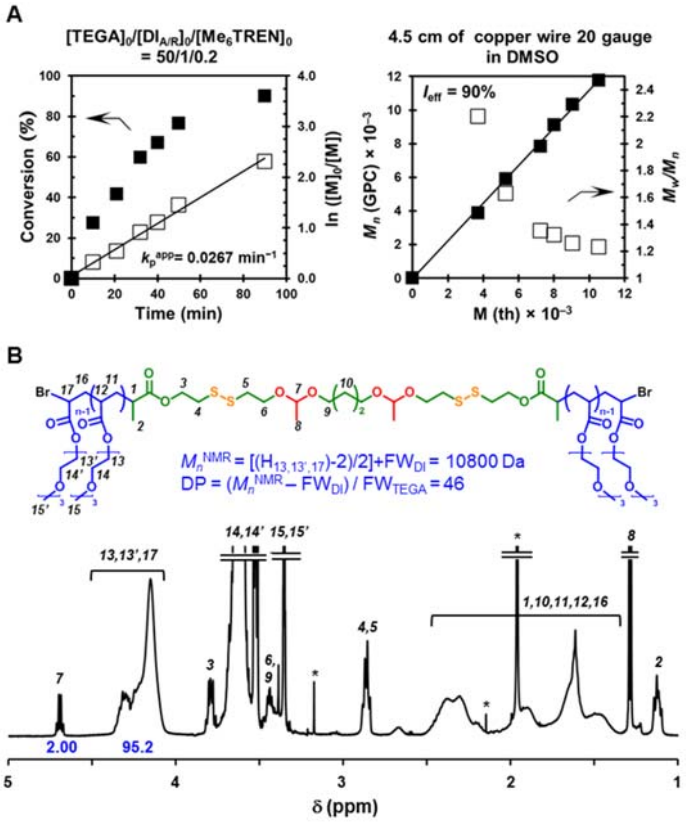

Figure 2. SET-LRP synthesis of ATHs from TEGA and DI$_{A/R}$. (A) Monomer conversion, kinetics plots, and evolution of experimental M_n(GPC) and M_w/M_n, based on the calibration by PMMA standards *vs* theoretical M(th) for the SET-LRP of TEGA initiated from DI$_{A/R}$ in DMSO. Reaction conditions: TEGA = 0.5 mL, DMSO = 0.25 mL, [TEGA]$_0$/[DI$_{A/R}$]$_0$/[Me$_6$-TREN]$_0$= 50/1/0.2, and 4.5 cm of the hydrazine-activated copper wire 20 gauge. (B) ^{1}H NMR spectrum of ATH2 in $CDCl_3$ (10 mg·mL^{-1}) at 25 ºC. ^{1}H NMR resonances from residual nondeuterated solvents are indicated with *.

The typical proton peaks of both pendant and main chain repeating unit structure, e.g. 4.0-4.5 ppm, and initiator residue integrating acetal, e.g. 1.1 ppm, and disulfide, e.g. 2.8 ppm, junctions were clearly observed, proving the successful polymerization. Furthermore, molecular weight and DP values of target ATHs, determined by comparing the ^{1}H NMR peak at 4.7, i.e. attributed to the acetal methine protons at the initiator residue, with those between 4.0-4.5 ppm, i.e. attributed to the polymer end and side groups, proved to be consistent with theoretical and GPC values (Figure 2B and Table 1). Finally, the symmetric architecture of the synthesized homopolymers was confirmed by conducting site-selective middle-chain

cleavage studies on the dissolved polymers under both acidic and reductive conditions (*vide infra*). Overall, these results demonstrated the successful synthesis of ATHs *via* SET-LRP.

Self-Assembly of ATHs in Aqueous Solutions. As detailed previously, hydrophilic homopolymers as well as random copolymers with either hydrophobic end(s)[13-17] or middle-groups[39,40] can self-assemble in aqueous solution into regular nanoassemblies, including micelles, vesicles and flower-like complex particles. In our case, the aggregation of folded ATH chains was expected to form in aqueous solutions micelle-like nanoassemblies with the dual acid pH and reduction-activated initiator residue serving as inner core and the hydrophilic poly(TEGA) arms as outer corona (Figure 1B).

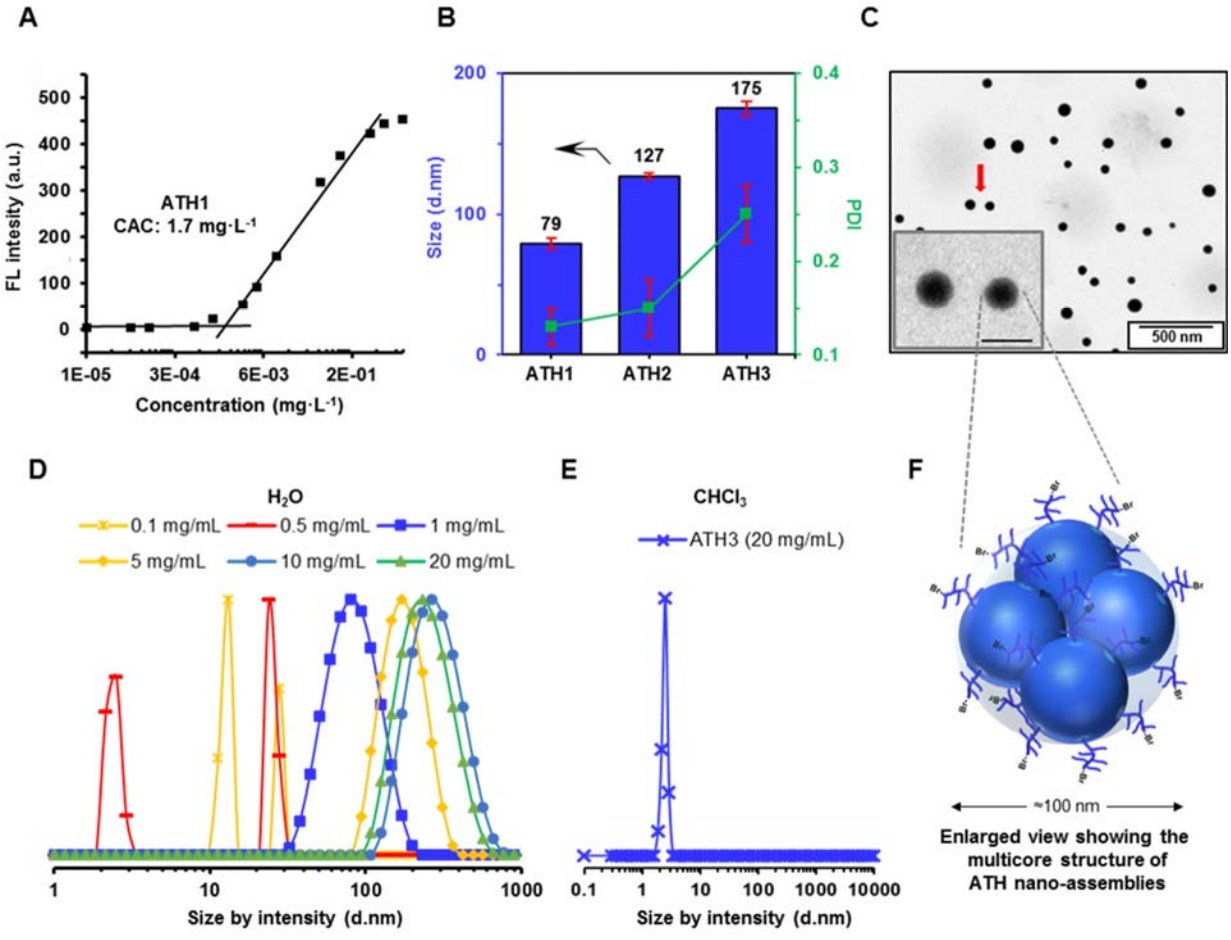

Figure 3. Self-assembly behavior of ATHs. (A) Plot of the fluorescence intensity from the NR emission at 625 nm (λ_{exc} = 550 nm) *vs* the logarithm of the ATH1 concentration. (B) DLS size and PDI for self-assembled ATHs in aqueous solution by nano-precipitation method (1 mg·mL^{-1}). (C) Non-stained TEM

image of ATH1 nanoassemblies (1 mg·mL^{-1}). Scale bar in the expansion is 100 nm. (D) DLS data for ATH1 nanoassemblies in aqueous solution as function of the polymer concentration (pH 7.4, 25 °C). (E) DLS data for ATH3 in $CHCl_3$ (1 mg·mL^{-1}). (F) Schematic illustration of the unimolecular multimicelle aggregates of ATH formed by aggregation of small micelles (the size of the small micelles is magnified).

As a first step in characterizing self-assembly behavior, CAC values were determined by fluorescent probe molecule method using Nile red.[49] As shown in Figure 3A, negligible fluorescence was detected at low polymer concentration, although suddenly an abrupt change in intensity was observed above a critical concentration, indicating the incorporation of the Nile red molecules into the hydrophobic core of the formed micelle-like nanoassemblies. Hence, ATH1 has a low apparent CAC of about 1.7 mg·L^{-1}. Interestingly, CAC values determined graphically from the intersection of the two lines appeared to be higher for homopolymers with longer poly(TEGA) segments due to a higher hydrophilic character (see Table 1). However, when considering the increase in molecular weight in ATH1-3, the CACs of the three homopolymers is relatively closer to each other. Next, the self-assembly of ATHs in aqueous solution was induced using a nano-precipitation method, i.e. slow-injection of water droplets into polymer in THF solution (THF/water ratio = 1/7), to obtain thermodynamically stable self-assembled nanostructures. The samples were prepared at 1 mg·mL^{-1}, which was a higher concentration than CAC. The hydrodynamic diameter (D_h) and morphology of the resulting nanoassemblies were characterized by dynamic light scattering (DLS) and transmission electron microscopy (TEM). As shown in Figure S6, ATH1 self-assembled into well-dispersed nanoparticles with an average diameter well-below 100 nm, i.e. D_h = 79 ± 0.4 nm and polydispersity index (PDI) = 0.13 ± 0.02. As expected, self-assembly of ATH1 could also be accomplished by direct dispersion in water, although this less time-consuming preparation led to slightly larger and broader particles (Figure S7). The size and PDI of the nanoassemblies increased with poly(TEGA) molecular weight because hydrophilic arms are extended in water (Figure 3B). Also TEM analyses demonstrated the formation of spherical nanoassemblies well-defined exterior boundary and a

slightly darker core (Figure 3C). However, the size of these nanoparticles is not in agreement with the presence of simple unimolecular micelles with homopolymer chains adopting a folded chain structure (Figure 1B). Further concentration-dependent measurements (0.1-20.0 $mg \cdot mL^{-1}$) pointed toward a transition from water-soluble single random coil chains to small unimolecular micelles which are just intermediates because further aggregate into unimolecular multimicelle aggregates with multi-core structure when increasing concentration (Figure 3D).[50-53] As a control, DLS analysis in a good organic solvent for both poly(TEGA) arms and initiator residue revealed the presence of single random coil chains with $D_h < 5$ nm rather than self-assembled nanostructures even at high concentration (Figure 3E). Since the weight fraction of the hydrophobic initiator residue in the whole hydrophilic ATHs is tiny while the amount of water is large, the high water's polarity and energy state of nanoparticles might be driving the assembly of single random coil chains into small micelles in state of high energy due to unfavorable amphiphilicity.[54] According to the fact that the larger particles are more energetically stable than the smaller ones,[55] these small micelles aggregate spontaneously until the size is large enough to make the formed nanoassemblies, i.e. unimolecular multimicelle aggregates, stable in the polar environment (Figure 3F). Inter-micellar interactions through hydrophilic coronas must also be contributing to the overall self-aggregation process.[56-58] This contribution is also reasonable based on the above mentioned observation that size of the nanoassemblies increased with increasing molecular weight of hydrophilic homopolymer (Figure 3B). ATHs with longer hydrophilic block lengths are more prone to form larger clusters, e.g. unimolecular multimicelle aggregates. Since the micellar self-assembly of this new class of amphiphilic homopolymers was demonstrated, we envisioned great potential scope in drug encapsulation and delivery because degradable acetal and disulfide functionalities were expected to act as a "keystone" for the particles under relevant biochemical conditions.

pH and Reduction-Triggered Breakdown of ATH Nanoassemblies. It is known that the acetal and disulfide linkages can be selectively and even orthogonally disconnected upon exposure to biologically relevant input signals, i.e. acidic pH and reductive conditions, respectively.[33,44,59] Accordingly, we expected that the decrease to half value in the molecular weight of ATHs upon site-selective cleavage at their core unit should dramatically impact their solubility behavior in aqueous solution.[39,40] To verify dual-responsive property, we monitored the stability of the ATH1 nanoassemblies under different biomimetic conditions by DLS (Figure 4A-C). Upon exposure to pH 7.4 buffer conditions similar to normal physiological environments, the nanoparticles showed remarkable dimensional stability and keep stable size around 80 nm for at least 12 h (Figure 4A). Stability in terms of nanoparticle morphology and size was also demonstrated by TEM (Figure S8). However, declining the pH value to 5.0, evidently activated the breakdown of the nanoassemblies (Figure 4B). DLS analysis revealed that complete dissolution of the particles occurred in a time scale of 12 h, which may be advantageous for designing sustained drug delivery at specific acidic sites, e.g. tumor tissues.[43] Interestingly, the breakdown of the self-assembled particles occurred through an increasing-decreasing profile (Figure S9), suggesting that it follows a swelling-to-crack mechanism driven by the acid hydrolysis of acetal linkages (Figure 4D). TEM was employed to visualize the remarkable expansion of the nanoassemblies (Figure S10). The cleavage of the acetal linkages was further demonstrated by GPC, because when the THF-dissolved symmetric polymer was treated with acid, a decrease in polymer size by a factor of two was observed with retention of monomodality and narrow molecular weight distribution, indicating the site-selective disconnection of the two-arm homopolymer into two equally sized fragments (Figure 4E).[42]

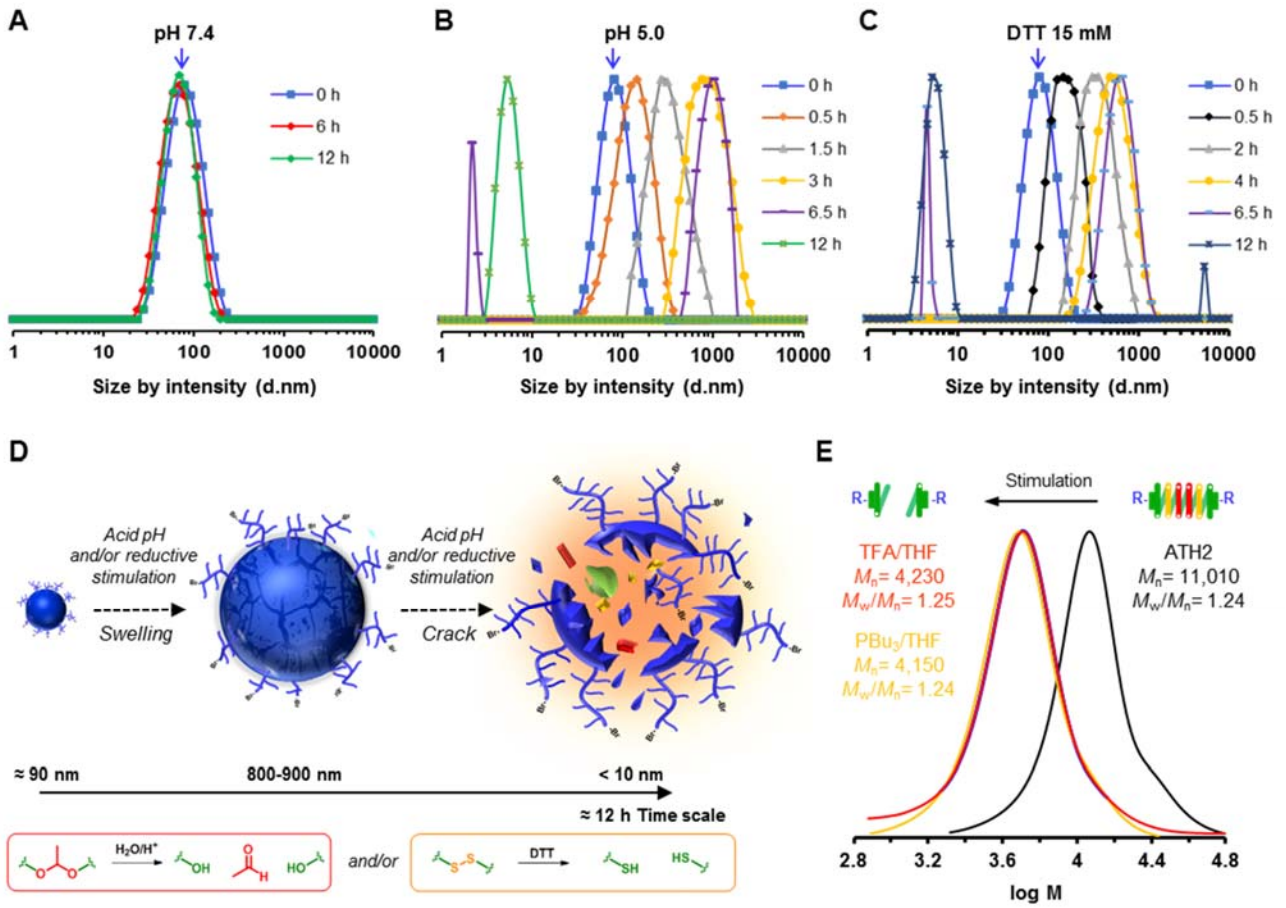

Figure 4. pH- and reduction-triggered breakdown of ATH nanoassemblies. (A) Size change through time of ATH1 nanoassemblies in response to (A) pH 7.4, (B) acid pH treatment (pH 5.0) and (C) reductive treatment (15 mM DTT). DLS traces at t_0 are indicated by blue arrows. (D) Schematic of pH/reduction dual-triggered "swell-crack" breakdown of ATH nanoassemblies *via* cleavage of acetal and/or disulfide linkages. (E) GPC traces for ATH2 dissolved in THF before (black line) and after either acidic pH (0.1 M trifluoroacetic acid, red line) or reductive (100 equiv. PBu_3, orange line) treatments. Both treatments were conducted for 60 min to promote middle-chain cleavage of the telechelic architecture. Note that the polymer chains in schematic illustrations shown in panel E are indicated with (-R) for simplicity.

This is an additional prove of the symmetric telechelic structure of the synthesized polymers. When a colloidal dispersion comprising ATH1 nanoassemblies was treated with DTT (15 mM), the size of nanoparticles also markedly enlarged prior breakdown into soluble unimers of < 10 nm, demonstrating the cleavage of disulfide bonds and the dissociation of the aggregation under reductive conditions (Figure 4C and S9). Nanoassemblies size expansion occurring upon reductive stimulation was also confirmed by

TEM (Figure S11). Reductive splitting of the dissolved telechelic polymer was further demonstrated by GPC (Figure 4E). Overall, DLS and GPC measurements clearly demonstrate the favorable dual pH and reduction responsive self-assembly behavior of the conceived simple ATH nanoassemblies, making these materials appealing for the design and preparation of anti-tumor drug carriers for cancer therapy owing to the fact that tumor cells and tissues show low pH and a high reducing environment.[35,45]

Drug Release Profiles from ATH Nanoassemblies. The potential of ATH1 nanoassemblies to load and deliver hydrophobic chemotherapeutic agents was investigated using CC as a model hydrophobic drug (Figure 5A). This polyphenolic compound, chemically identified as (1E,6E)-1,7-bis (4-hydroxy-3-methoxyphenyl)-1,6-heptadiene-3,5-dione, is a popular pleiotropic active agent due to its plenty therapeutic properties,[60] among them the ability to induce selective apoptosis to various tumor cells.[61,62]

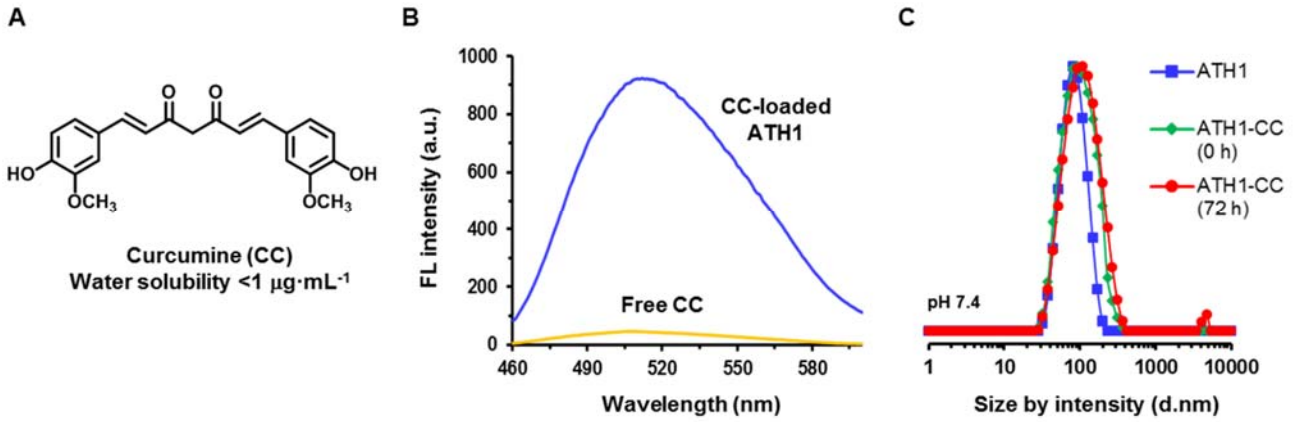

Figure 5. Encapsulation of hydrophobic CC drug into ATH1 nanoassemblies. (A) Chemical structure of CC. (B) Fluorescence spectrum of CC-loaded ATH1 nanoassemblies and free CC in aqueous solutions at equivalent concentrations of drug. (C) DLS measurements to study the stability of CC-loaded ATH1 nanoassemblies (1 mg polymer·mL^{-1}) at pH 7.4. Data for non-loaded particles is included for comparison purposes.

The extremely low aqueous solubility of this drug (<1 µg·mL^{-1}) as well as instability at physiological pH has stimulated the intensive search of nano-sized vehicles for efficient intracellular CC delivery.[30,62-64]

Herein, CC-loaded nanoassemblies were prepared by conano-precipitation starting from a solution containing both amphiphilic homopolymer (ATH1) and hydrophobic drug (CC) (see experimental section for details). We first confirmed the non-covalent encapsulation of CC *via* fluorescence spectroscopy analysis of the obtained bright yellow aqueous colloidal solution. As can be seen in Figure 5B, the poorly water-soluble CC only showed its characteristic intense emission peak at 516 nm when loaded into the hydrophobic cores of the nanoparticles. Note that the CC loading content and encapsulation efficiency values achieved with our designed amphiphilic homopolymer, i.e. 8.1 and 81.0%, respectively, are highly competitive compared to other CC carriers based on block copolymers.[30,64] After drug encapsulation, DLS analysis revealed a slight particle expansion (from 79 to 95 nm) which is consistent with the entrapment of the drug into the core reservoir of the nanoassemblies (compare squares and diamonds in Figure 5C). The prepared CC-loaded nanoparticles demonstrated to be stable for at least 72 h (circles in Figure 5C).

Next, we turned to evaluate the *in vitro* acid-triggered release of CC from the loaded nanoassemblies by tracing its fluorescent intensity upon exposure to the following conditions: pH ranging from 5.0 to 7.4 or 5.0 to 15.0 mM DTT. Note that for efficient anti-tumor drug delivery systems, nanocarriers are expected to be stable during circulation in the blood while also releasing the encapsulated drugs rapidly after entering the tumor cells. Preliminary control experiments demonstrated negligible CC release under conditions mimicking normal physiological environment (PBS, pH 7.4) (diamonds in Figure 6A). However, as shown in Figure S12, a progressive decrease of fluorescence intensity occurred throughout the incubation at pH 5.0. Under these conditions, the ultimate release value (URV) after 11 h was about 93% (circles in Figure 5A).

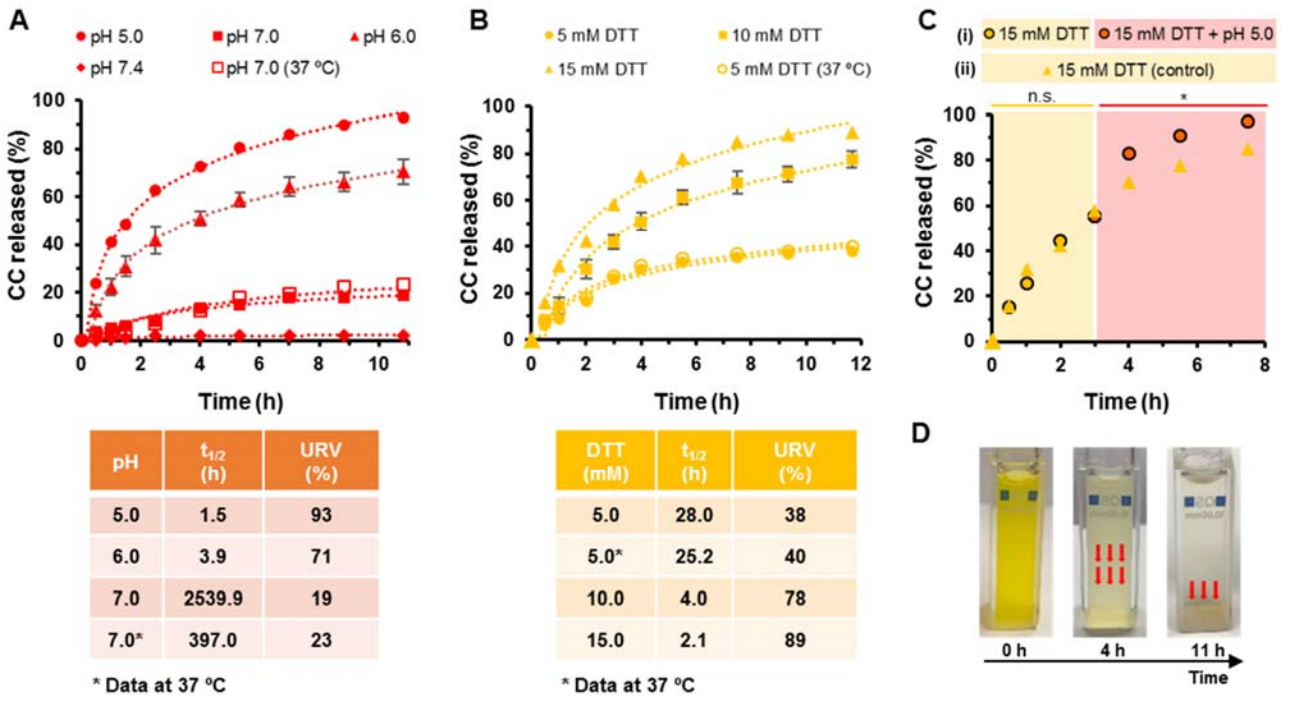

pH	$t_{1/2}$ (h)	URV (%)
5.0	1.5	93
6.0	3.9	71
7.0	2539.9	19
7.0*	397.0	23

* Data at 37 °C

DTT (mM)	$t_{1/2}$ (h)	URV (%)
5.0	28.0	38
5.0*	25.2	40
10.0	4.0	78
15.0	2.1	89

* Data at 37 °C

Figure 6. ***In vitro*** **release of CC from ATH1 nanoassemblies.** (A) CC release profile from ATH1 nanoassemblies in aqueous solution (1 mg polymer·mL^{-1}) in response to various pHs. (B) CC release profile from ATH1 nanoassemblies in aqueous solution (1 mg polymer·mL^{-1}) in response to various DTT concentrations. The dotted lines in A and B are the logarithmic fitting curves of the data points, $t_{1/2}$ is the half-release time of CC, and URV is the ultimate release value at the end of each drug release experiment. All the experiments were conducted at 25 ºC unless otherwise noted. (C) CC release profile from ATH1 nanoassemblies in aqueous solution (1 mg polymer·mL^{-1}) in response to (i) reductive-acid sequential additive (15 mM DTT for 3 h and 15 mM DTT/pH 5.0 for 5 h) and (ii) control 15 mM DTT (8 h) treatments. Both treatments are not statistically significantly from each other during the first 3 h (n.s., two-way ANOVA without replication) but are significantly different once pH is reduced to 5.0 in treatment (i) (*p-value = 0.002). (D) Representative digital images taken at different times during the release of CC from ATH1 nanoassemblies.

As expected, the release kinetics decreased with increasing pH of the soak-buffer.[59] For instance, release rate decreased by a factor of around 2 times when the pH was increased from 5.0 to 6.0. However, it is noteworthy to mention that the system provided short half-release times ($t_{1/2}$) under conditions mimicking acidic intracellular environments inside endosome and lysosome (pH 4.5-6.5). Conversely, the CC release tended to equilibrium at about 20% at pH closer (pH 7.0) to that which is characteristic of extracellular healthy environments (pH 7.4). Note that data from an in vitro CC release experiment at 37 ºC was

comparable to that obtained at 25 ºC (compare solid and empty squares in Figure 6A). To validate reduction-triggered drug release, *in vitro* drug release behaviors were also investigated in PBS (pH 7.4) in the presence of various concentration of DTT. As shown in Figure 6B, the CC release rate in response to conditions mimicking intracellular tumor reductive microenvironments (10 mM DTT) was almost alike to that at pH 6.0 (compare triangles with squares in Figure 6A and B, respectively). Incubation with 15 mM DTT further accelerated the drug release. Under these conditions, almost 90% of loaded CC was released from the nanoassemblies ($t_{1/2}$ = 2.1 h). However, a very slow release was observed with 5 mM DTT just reaching about 40% in 12 h both at room temperature (25 ºC) and at body temperature (37 ºC) (filled and empty circles in Figure 6B). Furthermore, fine-tuned release modes were also accessible under co-triggered conditions. As can be seen in Figure 6C, improved release character was observed under the effect of dual factors when applying simultaneously reductive and acid treatments (15 mM DTT and pH 5.0) after a short period of exclusive reductive stimulation. The same protocol can be applied starting first with acidic conditions (Figure S13). Throughout all these *in vitro* drug release studies, the CC release process could also be visually monitored because the experiment solution progressively turned from bright yellow to colorless while poorly water-soluble CC precipitated at the bottom of the cuvette (Figure 6D). This series of experiments suggest that ATH1-CC nanoassemblies may rapidly release cargo in response to acid/reductive microenvironments proposedly during endocytosis into cancer cells.[65]

In vitro **Cytotoxicity and Cellular Uptake.** Encouraged by the above reported findings, we were interested in testing the potential of using our simple CC-loaded nanoparticles in living cells. Two cell lines, HeLa, a human cervix epithelioid carcinoma cell line, and HT-29, a human colon adenocarcinoma cell line, were used as models. Prior to assess the biological activity of the encapsulated CC, the effect of empty ATH1 nanoassemblies in cell viability was determined in both cell lines using CellTiter 96®

AQueous One Solution Cell Proliferation Assay Kit (Promega) as reactive. The homopolymer in study did not exhibit relevant toxic effects (>95% cell viability) up to a concentration of 300.0 $\mu g \cdot mL^{-1}$ (Figure 7A), a compound concentration which is considered enough to meet most drug delivery requirements.

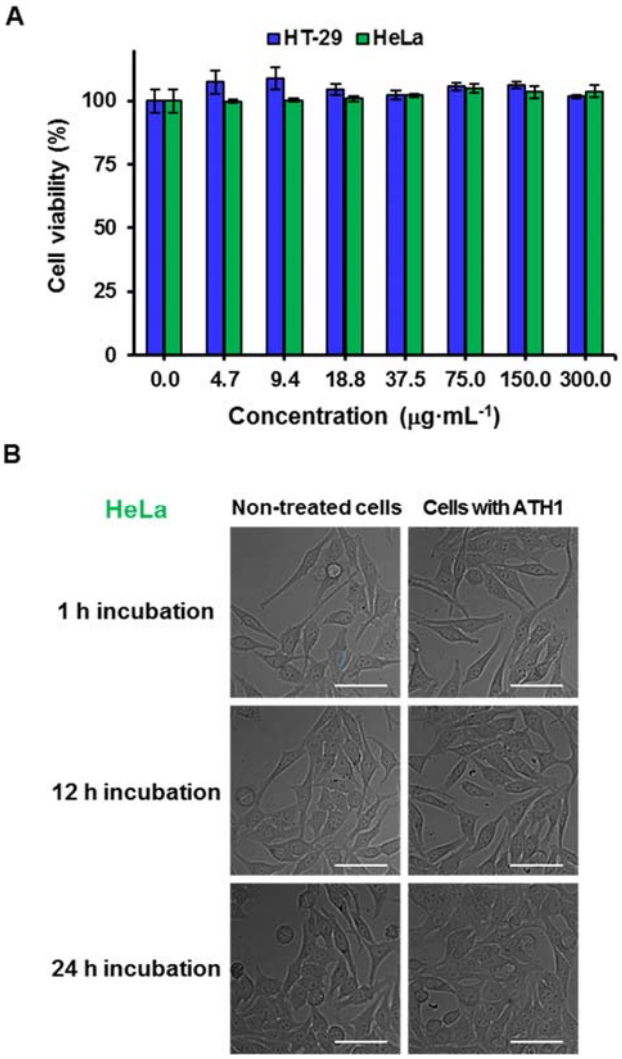

Figure 7. Cytotoxicity of empty ATH1 nanoassemblies against HT-29 and HeLa cell lines. (A) Cell viability values for HT-29 and HeLa cells determined by CellTiter 96® assay after 48 h of incubation with various concentration of empty ATH1 nanoassemblies. All the data are presented as the average ± standard deviation. (B) Confocal microscopy images of HeLa cell cultures non-treated and treated with ATH1 nanoassemblies. Images taken at different times (1 h, 12 h, and 24 h) at $[ATH1]_0$ = 120 $\mu g \cdot mL^{-1}$. Scale bars represent 100 μm.

Confocal microscopy images obtained during the cell culture were analyzed and the effect of assemblies on cell morphology was determined (Figure 7B and S12). In the presence of polymer (120 $\mu g \cdot mL^{-1}$) both cell lines showed normal proliferation with no changes in cell morphology when compared to non-treated cells (used as controls). For example, both non-treated and treated HeLa cells were adherent and exhibited their typical smooth surface and elongated structure (Figure 7B). No noticeable morphological changes were observed either in HT-29 line (Figure S14).

Next step, the effect of treating HT-29 and HeLa cells with CC-loaded ATH1 nanoassemblies in comparison to free CC was investigated. As shown in Figures 8A and B, half-maximal inhibitory concentration (IC50) of CC-ATH1 treatment was lower in comparison to free CC, which could be explained due to the enhanced aqueous solubility of CC in the nanoparticles in combination with accelerated acid/reductive-triggered release of CC in the tumor environment or after endocytosis in endosomes or lysosomes.[65] It is important to note that CC did not promote cytotoxicity in HT-29 line at a concentration below 16.8 $\mu g \cdot mL^{-1}$ (cell viability over 90%) but the IC50 of CC-loaded nanoassemblies was about 8.3 $\mu g \cdot mL^{-1}$ (Figure 8A). On the other hand, the CC-loaded ATH1 possessed over 2.7 fold lower IC50 value than free CC also for HeLa cell line (Figure 8B). These results demonstrate a greater effect in reducing initial cell viability percentage when cells are treated with the drug-loaded nanoformulation over free CC. As in the case of the empty assemblies, confocal microscopy was used to observe morphological changes in the cells at early stages of drug release process to provide qualitative information about the effect in cells. The green intrinsic fluorescence of CC seems to be detected after 1 h inside HT-29 cells after exposing to either CC-loaded nanoassemblies or free CC, suggesting that both systems undergo intracellular trafficking (Figure 8C).[66]

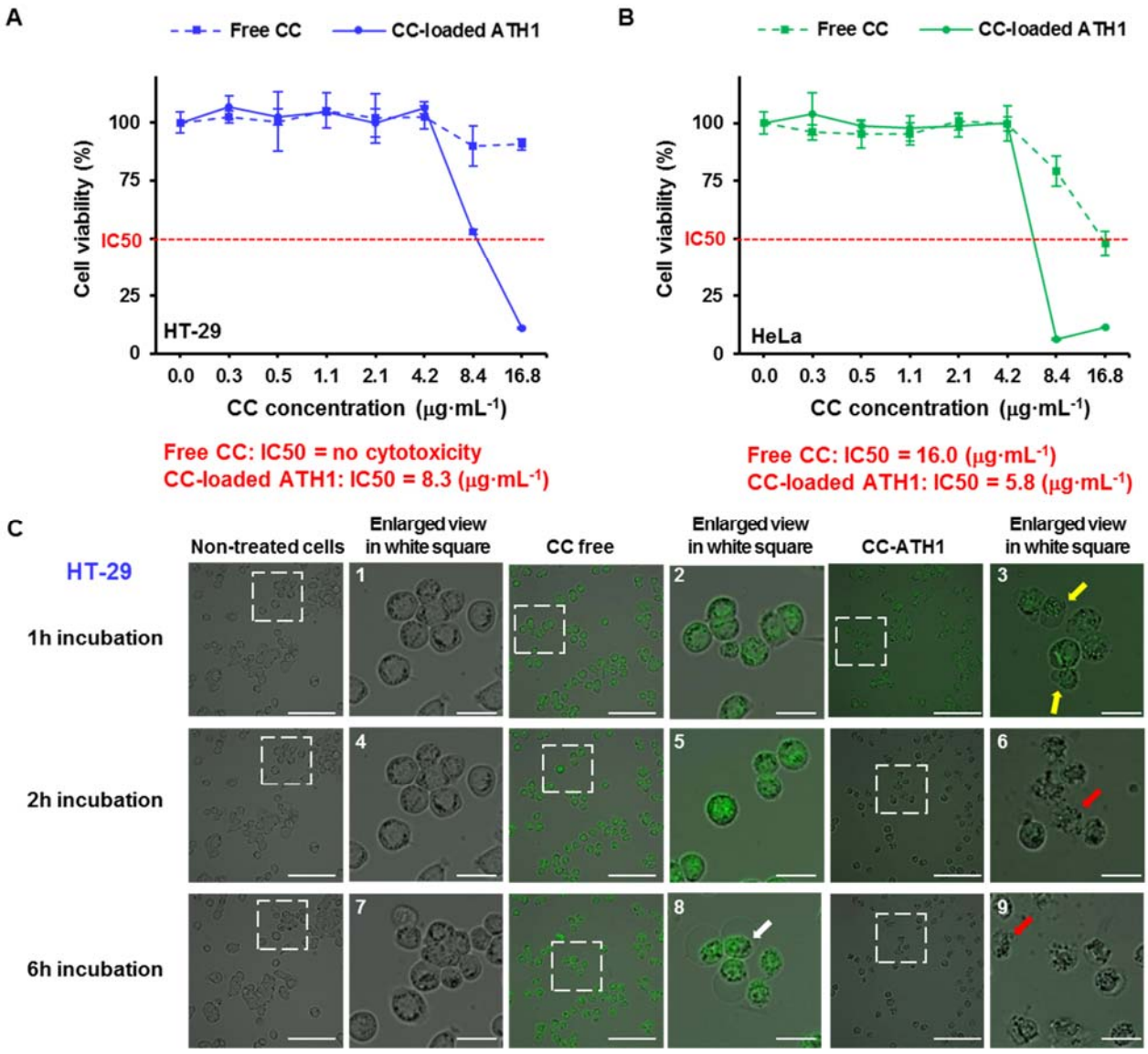

Figure 8. Cytotoxicity of CC-loaded ATH1 nanoassemblies against HT-29 and HeLa cells. Cell viability of HT-29 (A) and HeLa (B) cells after incubation with free CC and CC-loaded ATH1 nanoassemblies for 24 h at various CC concentrations. (C) Confocal images of HT-29 cells after incubation with free CC and CC-loaded ATH1 nanoassemblies for 1 h, 2 h, and 6 h ($[CC]_0$ = 6.7 μg·mL^{-1}). Images of non-treated cells are also shown for comparison purposes. White arrow in enlarged view 8 indicates cell shrinkage, yellow arrows in 3 indicate early apoptotic cells, and red arrow in 6 and 9 indicates nucleus fragmentation. Scale bars represent 100 μm (25 μm for the magnified sections).

HT-29 cells incubated with free drug retained the morphology of non-treated control cells and they only started to show overall shrinkage in their volume after 6 h (compare enlarged views 2, 5, and 8 with 1, 4,

and 7). White arrow in enlarged view 8 indicates early cell shrinkage. However, what is more interesting is that they conversely showed more premature suffering when treated with CC-loaded nanoparticles (see enlarged views 3, 6, and 9). Early apoptotic bodies indicated by yellow arrows in the enlarged view 3 were already observed after 1 h. Moreover, intense fragmentation indicated by red arrows was noted at longer exposure times. Fluorescence microscopy results for HeLa cells also revealed that the use of CC-loaded ATH1 nanoparticles induced greater morphological disruption than free CC (Figure S15). These observations are consistent with previous observations with other CC-loaded nanoparticles and cell lines.[30,64] Overall, it has been demonstrated that our design based on programmed associative homopolymers could be considered a particularly interesting simplified platform for cancer chemotherapy.

CONCLUSIONS

Fully hydrophilic telechelic dibromo polymers with hydrophobic initiator residues precisely located at the center of the polymer chain can directly self-assemble in water to form micelle-like nanoaggregates due to their amphiphilic nature.[39,40] Herein, SET-LRP served to grow biocompatible poly(TEGA)s chains from an designed α-haloester type sequence-encoded DI containing both acetal and disulfide bonds. With the initiator residue forming the core of these simple nano-scaled assemblies, the combination of CAC, DLS, GPC, TEM, and fluorescence spectroscopy measurements in simulated biochemical environments was used to demonstrate their breakdown along with the ongoing precise middle-chain cleavage. Accordingly, the *in vitro* drug release of CC was stimulated in both acid pH and reductive conditions as well as co-triggered environments. Afterwards, even though the homopolymers resulted non-cytotoxic, the corresponding CC-loaded nanoparticles displayed more efficient growth inhibition of HT-29 and HeLa cells than free CC. The potential rich chemistry of the cleavable groups in difunctional and multi-functional initiators for SET-LRP offers a useful Lego-type platform for fabrication of simple and smart

drug-delivery vehicles by exploring the use of alternative commercial and designed hydrophilic monomers[67,68] as well as exploiting the appealing high chain end fidelity of SET-LRP polymers.[69-71]

ASSOCIATED CONTENT

Materials and instrumentation, synthetic route for $DI_{A/R}$ experimental procedures, additional DLS curves for ATH nanoassemblies, evolution of DLS size as a function of time during the breakdown of nanoparticles, representative fluorescence spectra recorded during CC-release experiments, complementary confocal microscopy images captured cytotoxicity studies (PDF).

AUTHOR INFORMATION

Corresponding Author

* Gerard Lligadas. E-mail: gerard.lligadas@urv.cat

Author Contributions

The manuscript was written through contributions of all authors. All authors have given approval to the final version of the manuscript.

Notes

The authors declare no competing financial interest.

ACKNOWLEDGEMENTS

Spanish Ministerio de Ciencia, Innovación y Universidades through project MAT2017-82669-R (to G.L. and J.C.R) and FPI grant BES-2015-072662 (to A.M.) and the Serra Hunter Programme of the Government of Catalonia (to G.L.) are acknowledged for supporting and funding this work. Miguel Servet

Program from Instituto de Salud Carlos III (CPII13/00017 to O.A.); Fondo de Investigaciones Sanitarias from Instituto de Salud Carlos III, and European Union (ERDF/ESF, 'Investing in your future') (PI18/00343 to O.A.); Diputación General de Aragón (Predoctoral Research Contract 2019 to A.J-A., 'Digestive Pathology Group' B25_20R to O.A.); Centro de Investigación Biomédica en Red en Enfermedades Hepáticas y Digestivas (CIBERehd). V.P. gratefully acknowledges support from the National Science Foundation Grants DMR-1066116, DMR-1807127 and the P. Roy Vagelos Chair at the University of Pennsylvania.

References

(1) Men, Y.; Li, W.; Janssen, G. J.; Rikken, R. S. M.; Wilson, D. A. Stomatocyte in Stomatocyte: A New Shape of Polymersome Induced via Chemical-Addition Methodology. *Nano Lett.* **2018**, 18, 2081-2085.

(2) van Hest, J. C. M.; Delnoye, D. A. P.; Baars, M. W. P. L.; van Genderen, M. H. P.; Meijer, E. W. Polystyrene-Dendrimer Amphiphilic Block Copolymers with a Generation-Dependent Aggregation. *Science* **1995**, *268*, 1592-1595.

(3) Nyström, A. M.; Wooley, K. L. The Importance of Chemistry in Creating Well-Defined Nanoscopic Embedded Therapeutics: Devices Capable of the Dual Functions of Imaging and Therapy. *Acc. Chem. Res.* **2011**, *44*, 969-978.

(4) Ueda, M.; Hashidzume, A.; Sato, T. Unicore-Multicore Transition of the Micelle Formed by an Amphiphilic Alternating Copolymer in Aqueous Media by Changing Molecular Weight. *Macromolecules* **2011**, *44*, 2970-2977.

(5) Rodríguez-Hernández, J.; Chécot, F.; Gnanou, Y.; Lecommandoux, S. Toward 'Smart' Nano-Objects by Self-Assembly of Block Copolymers in Solution. *Prog. Polym Sci*. **2005**, *30*, 691-724.

(6) Vasilevskaya, V.; Govorun, E. N. Hollow and Vesicle Particles from Macromolecules with Amphiphilic Monomer Units. *Polym. Rev*. **2019**, *59*, 625-650.

(7) Zhang, J.; Liu, K.; Müllen, K.; Yin, M. Self-Assemblies of Amphiphilic Homopolymers: Synthesis, Morphology Studies and Biomedical Applications. *Chem. Commun.* **2015**, *51*, 11541-11555.

(8) Changez, M.; Kang, N. G.; Lee, C. H.; Lee, J. S. Reversible and pH-Sensitive Vesicles from Amphiphilic Homopolymer Poly(2-(4-vinylphenyl)pyridine). *Small* **2010**, 6, 63-68.

(9) Wang, Y.; Alb, A. M.; He, J.; Grayson, S. M. Neutral Linear Amphiphilic Homopolymers Prepared by Atom Transfer Radical Polymerization. *Polym. Chem.* **2014**, *5*, 622-629.

(10) Savariar, E. N.; Aathimanikandan, S. V.; Thayumanavan, S. Supramolecular Assemblies from Amphiphilic Homopolymers: Testing the Scope. *J. Am. Chem. Soc.* **2006**, *128*, 16224-16230.

(11) Zhu, Y.; Liu, L.; Du, J. Probing into Homopolymer Self-Assembly: How Does Hydrogen Bonding Influence Morphology?. *Macromolecules* **2013**, 46, 194-203.

(12) Mane, S. R.; Rao N, V.; Chaterjee, K.; Dinda, H.; Nag, S.; Kishore, A.; Sarma, J. D.; Shunmugam, R. Amphiphilic Homopolymer Vesicles as Unique Nano-Carriers for Cancer Therapy. *Macromolecules* **2012**, *45*, 8037-8042.

(13) Zhang, J.; You, S.; Yan, S.; Müllen, K.; Yang, W.; Yin, M. pH-Responsive Self-Assembly of Fluorophore-Ended Homopolymers. *Chem. Commun.* **2014**, *50*, 7511-7513.

(14) Liu, T.; Tian, W.; Zhu, Y.; Bai, Y.; Yana, H.; Du, J. How Does a Tiny Terminal Alkynyl End Group Drive Fully Hydrophilic Homopolymers to Self-Assemble Into Multicompartment Vesicles and Flower-Like Complex Particles?. *Polym. Chem*. **2014**, 5, 5077-5088.

(15) Du, J.; Willcock, H.; Patterson, J. P.; Portman, I.; O'Reilly, R. K. Self-Assembly of Hydrophilic Homopolymers: A Matter of RAFT End Groups. *Small* **2011**, *7*, 2070-2080.

(16) Patterson, J. P.; Kelley, E. G.; Murphy, R. P.; Moughton, A. O.; Robin, M. P.; Lu, A.; Colombani, O.; Chassenieux, C.; Cheung, D.; Sullivan, M. O.; Epps, III, T. H.; O'Reilly, R. K. Structural Characterization of Amphiphilic Homopolymer Micelles Using Light Scattering, SANS, and Cryo-TEM. *Macromolecules* **2013**, *46*, 6319-6325.

(17) Xu, J.; Tao, L.; Boyer, C.; Lowe, A. B.; Davis, T. P. Facile Access to Polymeric Vesicular Nanostructures: Remarkable ω-End group Effects in Cholesterol and Pyrene Functional (Co)Polymers. *Macromolecules* **2011**, 44, 299-312.

(18) Ramireddy, R. R.; Prasad, P.; Finnea, A.; Thayumanavan, S. Zwitterionic Amphiphilic Homopolymer Assemblies. *Polym. Chem*. **2015**, *6*, 6083-6087.

(19) He, H.; Liu, B.; Wang, M.; Vacheta, R. W.; Thayumanavan, S. Sequential Nucleophilic "Click" Reactions for Functional Amphiphilic Homopolymers. *Polym. Chem*. **2019**, *10*, 187-193.

(20) Sun, H.; Fan, L.; Zou, K.; Zhu, H.; Du, J. Decoration of Homopolymer Vesicles by Antibacterial Ultrafine Silver Nanoparticles. *RSC Adv.* **2014**, *4*, 41331-41335.

(21) Mabire, A. B.; Robin, M. P.; Willcock, H.; Pitto-Barry, A.; Kirby, N.; O'Reilly, R. K. Dual Effect of Thiol Addition on Fluorescent Polymeric Micelles: ON-to-OFF Emissive Switch and Morphology Transition. *Chem. Commun*. **2014**, *50*, 11492-11495.

(22) Mane, S. R.; Rao N, V.; Shunmugam, R. Reversible pH- and Lipid-Sensitive Vesicles from Amphiphilic Norbornene-Derived Thiobarbiturate Homopolymers. *ACS Macro Lett.* **2012**, *1*, 482-488.

(23) Kubo, T.; Easterling, C. P.; Olsona, R. A.; Sumerlin, B. S. Synthesis of Multifunctional Homopolymers *via* Sequential Post-Polymerization Reactions. *Polym. Chem*. **2017**, *8*, 6028-6032.

(24) Mabire, A. B.; Brouard, Q.; Pitto-Barry, A.; Williams, R. J.; Willcock, H.; Kirby, N.; Chapman, E.; O'Reilly, R. K. CO_2/pH-Responsive Particles with Built-In Fluorescence Read-Out *Polym. Chem*. **2016**, *7*, 5943-5948.

(25) Hu, Z.; Jonas, A. M.; Varshney, S. K.; Gohy, J. F. Dilution-Induced Spheres-to-Vesicles Morphological Transition in Micelles from Block Copolymer/Surfactant Complexes. *J. Am. Chem. Soc*. **2005**, *127*, 6526-6527.

(26) Zhang, Q.; Lei, L.; Zhu, S. Gas-Responsive Polymers. *ACS Macro Lett.* **2017**, *6*, 515-522.

(27) Coumes, C.; Woisel, P.; Fournier, D. Facile Access to Multistimuli-Responsive Self-Assembled Block Copolymers *via* a Catechol/Boronic Acid Ligation. *Macromolecules* **2016**, *49*, 8925-8932.

(28) Herzberger, J.; Fischer, K.; Leibig, D.; Bros, M.; Thiermann, R.; Frey, H. Oxidation-Responsive and "Clickable" Poly(ethylene glycol) *via* Copolymerization of 2-(Methylthio)ethyl Glycidyl Ether. *J. Am. Chem. Soc.* **2016**, *138*, 9212-9223.

(29) Liu, X.; Zhu, J.; Ouyang, K.; Yan, Q. Peroxynitrite-Biosignal-Responsive Polymer Micelles as Intracellular Hypersensitive Nanoprobes. *Polym. Chem*. **2018**, *9*, 5075-5079.

(30) Zhao, J.; Wang, H.; Liu, J.; Deng, L.; Liu, J.; Dong, A.; Zhang, J. Comb-like Amphiphilic Copolymers Bearing Acetal-Functionalized Backbones with the Ability of Acid-Triggered Hydrophobic-to-Hydrophilic Transition as Effective Nanocarriers for Intracellular Release of Curcumin. *Biomacromolecules* **2013**, *14*, 3973-3984.

(31) Roy, D.; Brooks, W. L. A.; Sumerlin, B. S. New Directions in Thermoresponsive Polymers. *Chem. Soc. Rev.* **2013**, *42*, 7214 -7243.

(32) Han, D.; Tong, X.; Zhao, Y. Block Copolymer Micelles with Dual-Stimuli-Responsive Core for Fast or Slow Degradation. *Langmuir* **2012**, *28*, 2327-2331.

(33) Wang, H.; Tang, L.; Tu, C.; Song, Z.; Yin, Q.; Yin, L.; Zhang, Z.; Cheng, J. Redox-Responsive, Core-Cross-Linked Micelles Capable of On-Demand, Concurrent Drug Release and Structure Disassembly. *Biomacromolecules* **2013**, *14*, 3706-3712.

(34) Schattling, P.; Jochuma, F. D.; Theato, P. Multi-Stimuli Responsive Polymers – the All-in-One Talents. *Polym. Chem*. **2014**, *5*, 25-36.

(35) Jazani, A. M.; Arezi, N.; Maruya-Li, K.; Jung, S.; Oh, J. K. Facile Strategies to Synthesize Dual Location Dual Acidic pH/Reduction-Responsive Degradable Block Copolymers Bearing Acetal/Disulfide Block Junctions and Disulfide Pendants. *ACS Omega* **2018**, *3*, 8980-8991.

(36) Percec, V.; Guliashvili, T.; Ladislaw, J. S.; Wistrand, A.; Stjerndahl, A.; Sienkowska, M. J.; Monteiro, M. J.; Sahoo, S. Ultrafast Synthesis of Ultrahigh Molar Mass Polymers by Metal-Catalyzed Living Radical Polymerization of Acrylates, Methacrylates, and Vinyl Chloride Mediated by SET at 25 °C. *J. Am. Chem. Soc.* **2006**, *128*, 14156-14165.

(37) Lligadas, G.; Grama, S.; Percec, V. Single-Electron Transfer Living Radical Polymerization Platform to Practice, Develop and Invent. *Biomacromolecules* **2017**, *18*, 2981-3008.

(38) Anastasaki, A.; Nikolaou, V.; Haddleton, D. M. Cu(0)-Mediated Living Radical Polymerization: Recent Highlights and Applications: a Perspective. *Polym. Chem.* **2016**, *7*, 1002-1026.

(39) Moreno, A.; Ronda, J. C.; Cádiz, V.; Galià, M.; Lligadas, G.; Percec, V. pH-Responsive Micellar Nanoassemblies from Water-Soluble Telechelic Homopolymers Endcoding Acid-Labile Middle-Chain Groups in Their Hydrophobic Sequence-Defined Initiator Residue. *ACS Macro Lett.* **2019**, *8*, 1200-1208.

(40) Moreno, A.; Ronda, J. C.; Cádiz, V.; Galià, M.; Percec, V.; Lligadas, G. Programmed Self-Assembly and Stimuli-Triggered Response of Hydrophilic Telechelic Polymers with Sequence-Encoded Hydrophobic Initiators. *Macromolecules* **2020**, DOI: 10.1021/acs.macromol.0c01400.

(41) Delplace, V.; Nicolas, J. Degradable Vinyl Polymers for Biomedical Applications. *Nat. Chem*. **2015**, *7*, 771-784.

(42) Moreno, A.; Ronda, J. C.; Cádiz, V.; Galià, M.; Lligadas, G.; Percec, V. SET-LRP from Programmed Difunctional Initiators Encoded with Double Single-Cleavage and Double Dual-Cleavage Groups. *Biomacromolecules* **2019**, *20*, 3200-3210.

(43) Jazani, A. M.; Oh, J. K. Dual Location, Dual Acidic pH/Reduction-Responsive Degradable Block Copolymer: Synthesis and Investigation of Ketal Linkage Instability under ATRP Conditions. *Macromolecules* **2017**, *50*, 9427-9436.

(44) Du, J.; Choi, B.; Liu, Y.; Feng, A.; Thang, S. H. Degradable pH and Redox Dual Responsive Nanoparticles for Efficient Covalent Drug Delivery. *Polym Chem.* **2019,** *10*, 1291-1298.

(45) Li, D.; Bu, Y.; Zhang, L.; Wang, X.; Yang, Y.; Zhuang, Y.; Yang, F.; Shen, H.; Wu, D. Facile Construction of pH- And Redox-Responsive Micelles From a Biodegradable Poly(β-hydroxyl Amine) for Drug Delivery. *Biomacromolecules* **2016**, *1*, 291-300.

(46) Yin, Y.; Huang, X.; Lv, C.; Wang, L.; Yu, S.; Luo, Q.; Xu, J.; Liu, J. Construction of an Artificial Glutathione Peroxidase Active Site on Copolymer Vesicles. *Macromol. Biosci.* **2010**, *10*, 1505-1516.

(47) Syrett, J. A.; Jones, M. W.; Haddleton, D. M. A Facile Route to End-Functionalised Polymers Synthesised by SET-LRP *via* a One-Pot Reduction/Thiol-ene Michael-Type Addition. *Chem. Commun.* **2010**, *46*, 7181-7183.

(48) Rosen, B. M.; Jiang, X.; Wilson, C. J.; Nguyen, N. H.; Monteiro, M. J.; Percec, V. The Disproportionation of Cu(I)X Mediated by Ligand and Solvent into Cu(0) and Cu(II)X_2 and its Implications for SET-LRP. *J. Polym. Sci., Part A: Polym. Chem.* **2009**, *47*, 5606-5628.

(49) Gillies, E. R.; Jonsson, T. B.; Fréchet, J. M. J. Stimuli-Responsive Supramolecular Assemblies of Linear-Dendritic Copolymers. *J. Am. Chem. Soc.* **2004**, *126*, 11936-11943.

(50) Zhang, L.; Eisenberg, A. Multiple Morphologies of "Crew-Cut" Aggregates of Polystyrene-b-poly(acrylic acid) Block Copolymers. *Science* **1995**, *268*, 1728-1731.

(51) Zhang, L.; Eisenberg, A. Multiple Morphologies and Characteristics of "Crew-Cut" Micelle-like Aggregates of Polystyrene-b-poly(acrylic acid) Diblock Copolymers in Aqueous Solutions. *J. Am. Chem. Soc.* **1996**, *118*, 3168-3181.

(52) Mai, Y.; Zhou, Y.; Yan, D. Synthesis and Size-Controllable Self-Assembly of a Novel Amphiphilic Hyperbranched Multiarm Copolyether. *Macromolecules* **2005**, *38*, 8679-8686.

(53) Qi, M.; Zhou, Y. Multimicelle Aggregate Mechanism for Spherical Multimolecular Micelles: from Theories, Characteristics and Properties to Applications. *Mater. Chem. Front.* **2019**, *3*, 1994-2009.

(54) Yao, Y.; Li, C.; Liu, F.; Zhao, P.; Gu, Z.; Zhang, S. Covalent Capture of Supramolecular Species in an Aqueous Solution of Water-Miscible Small Organic Molecules. *Phys. Chem. Chem. Phys.* **2019**, *21*, 10477-10487.

(55) Ratke, L.; Voorhees, P. W. Growth and Coarsening: Ost-Wald Ripening in Material Processing, Springer Science & Business Media, 2013.

(56) Cameron, N. S.; Corbierre, M. K.; Eisenberg, A. Asymmetric Amphiphilic Block Copolymers in Solution: a Morphological Wonderland. *Can. J. Chem*. **1999**, *77*, 1311−1326.

(57) Li, C.; Madsen, J.; Armes, S. P.; Lewis, A. L. A New Class of Biochemically Degradable, Stimulus-Responsive Triblock Copolymer Gelators. *Angew. Chem. Int. Ed.* **2006**, *118*, 3510–3513.

(58) Cheng, X.; Jin, Y.; Fan, B.; Qi, R.; Li, H.; Fan, W. Self-Assembly of Polyurethane Phosphate Ester with Phospholipid-Like Structures: Spherical, Worm-Like Micelles, Vesicles, and Large Compound Vesicles. *ACS Macro Lett*. **2016**, *5*, 238-243.

(59) Liu, B.; Thayumanavan, S. Substituent Effects on the pH Sensitivity of Acetals and Ketals and Their Correlation with Encapsulation Stability in Polymeric Nanogels. *J. Am. Chem. Soc.* **2017**, *139*, 2306-2317.

(60) Gupta, S. C.; Patchva, S.; Aggarwal, B. B. Therapeutic Roles of Curcumine: Lessons Learned from Clinical Trials. *AAPS J.* **2013**, *15*, 195-218.

(61) Saheb, M.; Fereydouni, N.; Nemati, S.; Barreto, G. E.; Johnston, T. P.; Sahebkar, A. Chitosan-based Delivery Systems for Curcumin: A Review of Pharmacodynamic and Pharmacokinetic Aspects. *J. Cell. Physiol.* **2019**, *234*, 12325-12340.

(62) Salem, M.; Rohani, S.; Gillies, E. R. Curcumin, a Promising Anti-Cancer Therapeutic: a Review of its Chemical Properties, Bioactivity and Approaches to Cancer Cell Delivery. *RSC Adv*. **2014**, *4*, 10815-10829.

(63) Qiao, Z.; Liu, H. Y.; Zha, J. C.; Mao, X. X.; Yin, J. Completely Degradable Backbone-Type Hydrogen Peroxide Responsive Curcumin Copolymer: Synthesis and Synergistic Anticancer Investigation. *Polym Chem*. **2019**, *10*, 4305-4313.

(64) Raveendran, R.; Mullen, K. M.; Wellard, R. M.; Sharma, C. P.; Hoogenboom, R.; Dargaville, T. R. Poly(2-oxazoline) Block Copolymer Nanoparticles for Curcumin Loading and Delivery to Cancer Cells. *Eur. Polym. J*. **2017**, *93*, 682-694.

(65) Yin, Q.; Shen, J.; Zhang, Z.; Yu, H.; Li, Y. Reversal of Multidrug Resistance by Stimuli-Responsive Drug Delivery Systems for Therapy of Tumor. *Adv. Drug Delivery Rev*. **2013**, *65*, 1699-1715.

(66) Ghosh, M.; Ryan, R. O. Curcumin Homing to the Nucleolus: Mechanism for Initiation of an Apoptotic Program. *J. Nutr. Biochem.* **2014**, *25*, 1117-112.

(67) Miura Y. Synthesis and Biological Application of Glycopolymers. *J. Polym. Sci., Part A: Polym. Chem.* **2007**, *45*, 5031-5036.

(68) Bensabeh, N.; Moreno, A.; Roig, A.; Rahimzadeh, M.; Rahimi, K.; Ronda, J.C.; Cádiz, V.; Galià, M.; Percec, V.; Rodriguez-Emmenegger, C.; Lligadas, G. Photoinduced Upgrading of Lactic Acid-Based Solvents to Block Copolymer Surfactants. *ACS Sustain. Chem. Eng*. **2020**, *8*, 1276-1284.

(69) Rosen, B. M.; Lligadas, G.; Hahn, C. Percec, V. Synthesis of Dendritic Macromolecules through Divergent Iterative Thio-Bromo "Click" Chemistry and SET-LRP. *J. Polym. Sci., Part A: Polym. Chem.* **2009**, *47*, 3940-3948.

(70) Soeriyadi, A. H.; Boyer, C.; Nyström, F.; Zetterlund, P. B.; Whittaker, M. R. High-Order Multiblock Copolymers *via* Iterative Cu(0)-Mediated Radical Polymerizations (SET-LRP): Toward Biological Precision. *J. Am. Chem. Soc.* **2011**, *133*, 11128-11131.

(71) Beyer, V. P.; Cattoz, B.; Strong, A.; Phillips, D. J.; Schwarz, A.; Becer, C. R. Fast Track Access to Multi-Block Copolymers *via* Thiol-Bromo Click Reaction of Telechelic Dibromo Polymers. *Polym. Chem*. **2019**, *10*, 4259-4270.

“For Table of Contents Use Only”

Manuscript title: Dual Biochemically Breakable Drug Carriers from Programmed Telechelic Homopolymers

Authors: Adrian Moreno, Ana Jiménez-Alesanco, Juan C. Ronda, Virginia Cádiz, Marina Galià, Virgil Percec, Olga Abian, and Gerard Lligadas*

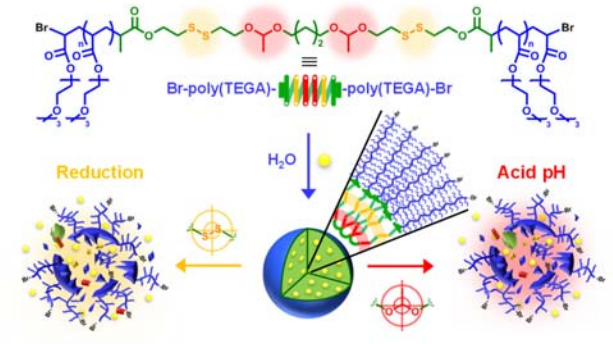

Table of Contents (TOC) Graphic